



Magnetic biochar-based manganese oxide composite for enhanced fluoroquinolone antibiotic removal from water

Ruining Li¹ · Zhaowei Wang¹ · Xiating Zhao¹ · Xi Li² · Xiaoyun Xie¹

Received: 1 March 2018 / Accepted: 24 August 2018 / Published online: 5 September 2018
© Springer-Verlag GmbH Germany, part of Springer Nature 2018

Abstract

Magnetic biochar-based manganese oxide composite (MMB) and raw biochar (BC) were synthesized via pyrolysis at a temperature of 500 °C under anoxic conditions of potato stems and leaves, characterized, and successfully used for the removal of norfloxacin (NOR), ciprofloxacin (CIP), and enrofloxacin (ENR) as representative compounds of fluoroquinolone antibiotics (FQs). Characterization results suggested that Fe₃O₄ and MnO_x are the dominant crystals in MMB. MMB possessed large surface area and pore volume than BC. Batch adsorption experiments showed that the maximum adsorption abilities of MMB for norfloxacin (NOR), ciprofloxacin (CIP), and enrofloxacin (ENR) were 6.94, 8.37, and 7.19 mg g⁻¹. In comparison to BC, the adsorption abilities of MMB increased 1.2, 1.5, and 1.6 times for NOR, CIP, and ENR, respectively. The pseudo-second-order kinetic model and the Langmuir model correlated satisfactorily to the experimental data. Thermodynamic studies revealed that the adsorption processes were spontaneous and endothermic. The adsorption capacity of MMB decreased with increasing solution pH (between 3.0 and 10.0) and increasing ionic strength (0.001–0.1). The MMB with high FQ removal efficiency, easy separation, and desirable regeneration ability may have promising environmental applications for the removal of fluoroquinolone antibiotics from water environment.

Keywords Biochar composite · Magnetic · Manganese oxide · Characterization · Fluoroquinolone antibiotics · Adsorption mechanism

Introduction

Fluoroquinolones (FQs) are a group of broad-spectrum antibiotics, commonly used in human and veterinary medicine (Huang et al. 2018; Wang et al. 2017a). FQs can be released into the aquatic environment due to incomplete metabolism in humans or coming from effluents of drug manufacturers (Van Doorslaer et al. 2014), and the residual FQs have been

frequently detected in the aquatic environment. Although their residual concentrations in environment are very low (ng·L⁻¹ to μg·L⁻¹) (Conkle et al. 2010; Peng et al. 2016), FQs have still attracted attention because of their potential risk to human health arising from increasing antibiotic-resistant bacteria over the long term. Therefore, FQ pollution in water is a necessary subject faced by environmental researchers.

Among many methods which were used to remove FQs from wastewater, adsorption is a top remediation technology because of its cost-effectiveness and easy operation (Luo et al. 2018; Solanki and Boyer 2017). FQ adsorptive removal studies are reported using several kinds of biochar materials (Rajapaksha et al. 2014; Yi et al. 2017). Biochar, a type of carbon-rich solid material, is derived from pyrolyzing biomass under elevated and oxygen-limited environment (Kumar et al. 2017). Biochar is widely used for favorable adsorbent due to its low cost, wide availability of feedstocks, and favorable physical/chemical surface characteristics (Kong et al. 2017; Peng et al. 2017; Tan et al. 2015). Unfortunately, one of the drawbacks of using biochar as an adsorbent is its difficulty in separating. So magnetic biochar has attracted broad attention

Responsible editor: Hailong Wang

Electronic supplementary material The online version of this article (<https://doi.org/10.1007/s11356-018-3064-1>) contains supplementary material, which is available to authorized users.

✉ Xiaoyun Xie
xiexiaoyun@lzu.edu.cn

¹ College of Earth and Environmental Sciences, Lanzhou University, Lanzhou 730000, China

² School of Public Health, Lanzhou University, Lanzhou 730000, China

in water treatment field which can easily be separated from water by an external magnetic field. Nevertheless, their efficient removal for many organic pollutants from water is still a challenge. Recently, some researchers have demonstrated that manganese oxide–modified biochar can improve pore properties of biochar and increase the oxygen-containing functionalities, thus it can strengthen the interactions between the biochar and pollutant (Fan et al. 2018; Li et al. 2017a). Herein, the new composite with magnetic biochar and MnO_x could integrate the advantages of easy separation, abundant functional groups, and large surface area. To the best of our knowledge, there have been very few studies on the adsorption of FQs with magnetic biochar-based manganese oxide composite. Consequently, it is attractive to understand the adsorption behavior and mechanism for the uptake of FQs by this cost-effective biochar composite.

The overall goal of this study, a novel manganese oxide–loaded magnetic biochar composite adsorbent was fabricated by impregnating KMnO_4 -coated magnetic biochar surface using simple methods. It can take merits of both the unique properties of magnetic biochar and manganese oxide–modified biochar. Furthermore, iron oxide and manganese oxide materials are widely found in the natural environment. Also, they were mostly investigated because of low cost and environmental friendliness. Thus, it could be a great potential and cost-effective adsorbent for removing FQs from water.

The adsorbents of raw biochar and novel magnetic biochar-based manganese oxide composite were tested

for ciprofloxacin (CIP), enrofloxacin (ENR), and norfloxacin (NOR), which are widely used fluoroquinolone antibiotics. The study objectives of our work were to (1) characterize the novel manganese oxide–loaded magnetic biochar composite and compare with raw biochar, (2) compare the adsorption ability of the biochar composite and raw biochar, and (3) evaluate the experiment parameters such as contact time, solution pH, temperature, initial concentration, ionic strength, and the regenerations.

Materials and methods

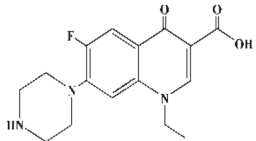
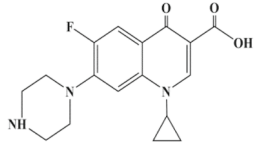
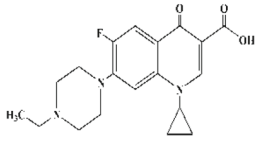
Chemical reagents

CIP, ENR, and NOR were purchased from J&K Scientific Ltd. (China). Its typical physicochemical properties are shown in Table 1. The chemicals employed in this study were of analytical grade. A stock solution of antibiotics ($10 \text{ mg}\cdot\text{L}^{-1}$) were prepared in ultra-pure water.

Preparation of biochar and magnetic biochar-based manganese oxide composite

Biochar was produced from potato stems and leaves through pyrolysis at $500 \text{ }^\circ\text{C}$ with a heating rate of $20 \text{ }^\circ\text{C min}^{-1}$ for 5 h and 35 min, and was abbreviated as BC. The manganese

Table 1 Physicochemical properties of three FQs

FQs	Molecular formula	Molecular weight($\text{g}\cdot\text{mol}^{-1}$)	pKa	Structure
NOR	$\text{C}_{16}\text{H}_{18}\text{FN}_3\text{O}_3$	319.33	pKa1=6.2 pKa2=8.5	
CIP	$\text{C}_{17}\text{H}_{18}\text{FN}_3\text{O}_3$	331.34	pKa1= 6.2 pKa2= 8.8	
ENR	$\text{C}_{19}\text{H}_{22}\text{FN}_3\text{O}_3$	359.46	pKa1=6.1 pKa2=7.7	

oxide-loaded magnetic biochar composite was obtained as follows:

1. 15.0 g biomass, 2.0 g sodium chloride, and 3.0 g ferric trichloride hexahydrate ($\text{FeCl}_3 \cdot 6\text{H}_2\text{O}$) were mixed with 60 mL high purified water and then dried at 80 °C. Then, the dried sample was pyrolyzed in identical fashion to BC. After being cooled, the sample was rinsed three times with diluted hydrochloride acid and highly purified water to thoroughly remove the external iron oxide and Fe. After drying, the sample was sieved with a sieve mesh of 0.15 mm and was referred as FB.
2. The MnO_x was loaded onto the FB with a weight ratio 1:10 in the following manner: 0.05 g KMnO_4 and 5.0 g FB sample were mixed with 40 mL high purified water. The suspension was ultrasonicated for 2 h and was then oven dried at 80 °C (Song et al. 2014). Then it was heated at 500 °C for 0.5 h under limited O_2 . The obtained sample was washed thoroughly with high purified water to remove impurities and dried at 80 °C. It was referred as MMB.

Characterization

Scanning electron microscope (SEM, JSM-5600LV; JEOL, Japan) was used to investigate the surface morphology of BC and MMB and localized elemental information was viewed with an energy-dispersive X-ray spectroscopy (EDS, IE250; Oxford Instruments, England) in conjunction with SEM. Fourier-transform infrared spectroscopy (FTIR, NEXUS 670; Thermo Fisher Nicolet, USA) was used to investigate their functional groups. The BET surface area (S_{BET}), pore volume, and pore size distribution of BC and MMB were determined by the BET adsorption method (Trustar II 3020; Micromeritics Instrument, USA). Point of zero surface charge (pH_{PZC}) was determined using the pH drift method (Carabineiro et al. 2011). Vibrating sample magnetometer (VSM, LAKESHORE-7304, USA) was employed to measure magnetism of MMB. Powder X-ray diffraction (XRD, D/max-2400, Japan) was employed to analyze the chemical composition of MMB. The chemical composition of the MMB was analyzed by X-ray photoelectron spectroscopy (XPS, PHI 5702, USA).

Adsorption experiment

All adsorption experiments were carried out in a 50-mL conical flask by adding 0.05 g of adsorbent with 25 mL antibiotic solution in a thermostatic shaker. Then 0.01 M CaCl_2 was added to the antibiotic solution to control the ionic strength during adsorption experiments. The kinetic data were generated by initial concentration of $10 \text{ mg} \cdot \text{L}^{-1}$ for antibiotic

solution. Adsorption isotherms data were obtained by performing the experiment at 15, 25, and 35 °C with the sample solution containing varying antibiotic concentrations in the range of 2, 5, 8, 10, 12, 14, and 16 $\text{mg} \cdot \text{L}^{-1}$ and the initial pH was adjusted to 3.0. The pH of the solution was adjusted by 0.1 M NaOH and HCl solution. All the tubes were sealed and shaken at 200 rpm for 24 h in the dark at 25 °C to reach apparent equilibrium based on the preliminary study. The effect of ionic strength on the experiments was studied by adding CaCl_2 to antibiotic solution with concentrations in the range of 0.001, 0.01, and 0.1 M at pH 3.0 at 25 °C.

Analytical methods

The concentrations of CIP, ENR, and NOR solution were measured by a UV-vis spectrophotometer (UNICAM UV300; Thermo Spectronic, USA) at 272, 270, and 273 nm. HPLC analysis for CIP, ENR, and NOR in water were quantified by HPLC with UV/visible and photodiode array detectors (Ultimate 3000; Thermo Spectronic, USA). The UV detection of CIP, ENR, and NOR were performed at 272, 270, and 273 nm. The analytical column was ZORBAX-C18 (250 mm × 4.6 mm, 5 μm). The temperature of the column was set at 30 °C. The mobile phase consisted of water (solvent A) and acetonitrile containing 0.2% methane acid (solvent B), and the volume ratio of solvent A and solvent B was 81:19.

The same adsorption experiments were repeatedly carried out two times under identical conditions. Control experiments without adsorbents were carried out in order to determine the adsorption of CIP, ENR, and NOR onto the surfaces of conical flask. The removal rate and adsorption capacity of CIP, ENR, and NOR on BC and MMB were computed by the following equations (Chen et al. 2017):

$$\text{Removal}(\%) = (c_0 - c_e) \times 100 / c_0 \quad (1)$$

$$q_e = (c_0 - c_e)v/m \quad (2)$$

where C_0 and C_e ($\text{mg} \cdot \text{L}^{-1}$) are the FQ initial and equilibrium adsorption concentrations, respectively. q_e ($\text{mg} \cdot \text{g}^{-1}$) is the amount of FQs adsorbed per unit mass of the adsorbent at equilibrium, v (L) is the volume of the FQ solution, and m (g) is the dose of adsorbent added to the solution.

Regeneration

The regeneration method was based on a previous study (Wu et al. 2005). Basically, the regeneration of MMB containing antibiotics was carried out by thermal degradation. After separation, the collected samples were dried at 80 °C, then placed into a muffle furnace and heated at 500 °C for 30 min. After that, the regenerated adsorbents were used in further experiments.

Results and discussion

Characterization of BC and MMB

SEM-EDS of BC and MMB are shown in Fig. 1. BC and MMB retain their physical form of their biomass precursor in Fig. 1a and b. Figure 1a shows that the BC surface is smooth, while MMB has a rougher surface than the BC (Fig. 1b). This might be that MnO_x is covered onto BC or iron oxide embedded in BC which changed the surface fabrication.

EDS elemental analysis confirmed the element existence of Mn and Fe on MMB, and the atomic ratio of Mn and Fe was about 0.40 on MMB. EDS mapping was further applied to investigate the elemental distribution throughout the MMB, and it showed that Mn and Fe had a similar elemental distribution pattern in MMB, supporting the conclusion that manganese oxide and iron oxide were formed in MMB.

XPS was used to characterize the chemical composition and metallic state of the MMB samples in Fig. 2. It can be noticed that an obvious increase of Fe2_p and Mn2_p intensity

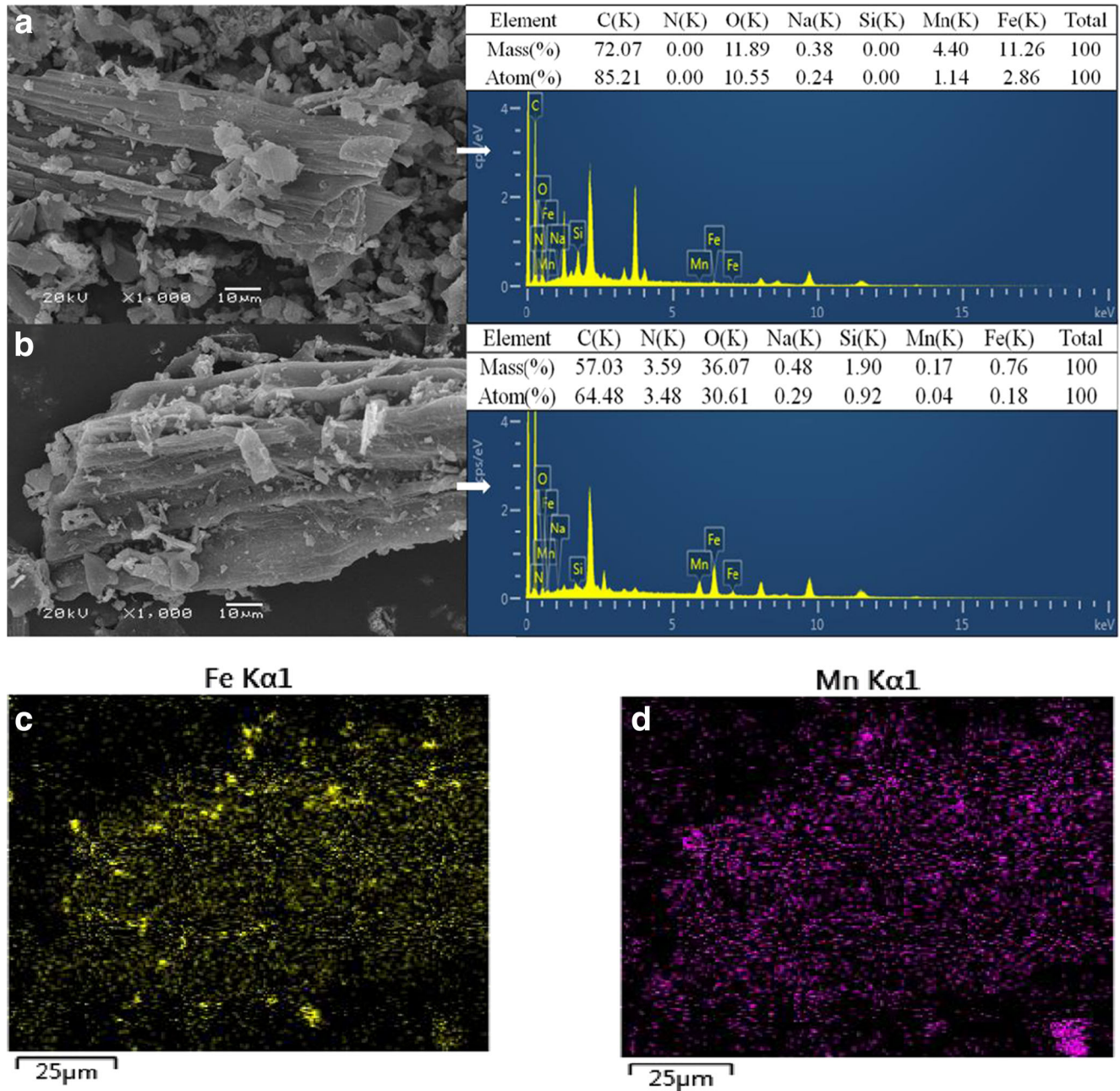


Fig. 1 SEM/EDS elemental mapping analysis for BC and MMB (surface topography of BC (a) and MMB (b) and corresponding EDS spectra with elemental ratio, Fe (c) and Mn (d) distribution map)

was observed from MMB in Fig. 2a, which is consistent with the EDS analysis results. To further describe the relative contents, Mn_{2p}, Fe_{2p}, and O1s spectra are present in Fig. 2b–d. As shown in Fig. 2b, the peaks of Mn_{2p_{3/2}} at 641.1 eV are characteristic peaks of MnO_x (Zhao et al. 2016), and the separation between Mn_{2p_{3/2}} and Mn_{2p_{1/2}} peaks is about 11.7 eV, indicating that Mn exhibits oxidation state between Mn³⁺ and Mn⁴⁺, and it can be seen to show Mn⁴⁺ predominantly from the Mn_{2p_{3/2}} peaks (Han et al. 2006). Figure 2c shows the XPS spectrum of Fe_{2p} of MMB. The peaks at 710.4 and 723.0 eV are indicative of Fe²⁺ while the peaks at 711.5 and 725.0 eV are indicative of Fe³⁺ on the MMB surface (Khmeleva et al. 2005; Zhao et al. 2016). The O1_s XPS spectrum (Fig. 2d) shows a large peak, which is a sum of the two peaks at 530.4 and 532.4 eV (Han et al. 2006; Ueda Yamaguchi et al. 2016). The peak at 530.4 eV is ascribed to the lattice oxygen of the metal oxides (Fe–O and Mn–O of the MMB sample) (Ueda Yamaguchi et al. 2016), the other peak at

532.4 eV can be assigned to hydroxyl on the MMB surface (C–OH) as well as chemisorbed water (Song et al. 2014).

The XRD of the MMB and BC are shown in Fig. S1. In contrast to the XRD pattern of MMB and BC, the former appeared the typical diffraction peaks at 18.5°, 30.5°, 35.3°, 43.3°, 53.9°, 57.3°, and 62.8° that corresponded to the (111), (220), (311), (400), (422), (511), and (440) planes of the Fe₃O₄.

The BET surface area of the MMB was about 2.54 times that in BC in Table 2. This may be due to the immobilization of MnO_x on the biochar surface which provides the additional surface area (Li et al. 2017a, b). Total pore volume and the micropore volume of MMB increased from Table 2. The average pore diameter of the MMB was found to be 2.56 nm which decreased in comparison to BC. These changes including pore volume and surface area in MMB promote the diffusion of FQs into these pores, thereby enhancing the adsorption capacity, which would likely be one of the mechanisms

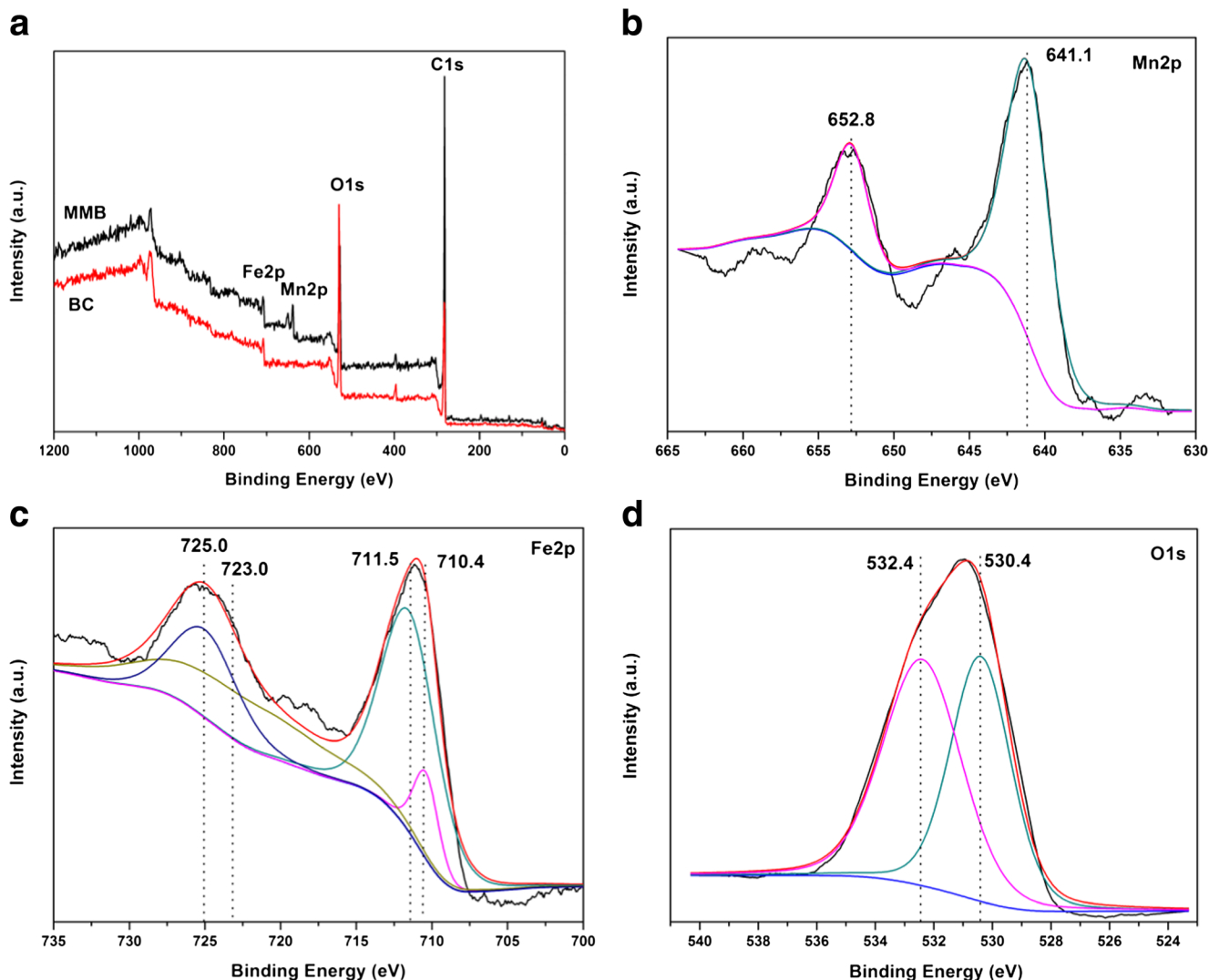


Fig. 2 a Wide-scan XPS spectra of BC and MMB; b Mn_{2p}, c Fe_{2p}, and d O1_s XPS spectra of MMB

Table 2 Physical character parameters of BC and MMB

Adsorbents	S_{BET} (cm ² ·g ⁻¹)	V_{total} (cm ³ ·g ⁻¹)	V_{micro} (cm ³ ·g ⁻¹)	D^a (nm)	Point of zero charge
BC	99.43	0.078	0.029	3.12	9.82
MMB	252.00	0.16	0.076	2.56	6.52

^a The average pore size

involved in the increased FQ adsorption by immobilizing of the Fe₃O₄ and MnO_x with biochar (Rajapaksha et al. 2014). The pH_{PZC} values of MMB and BC were measured to be 6.52 and 9.82 (Fig. S2) by using pH drift method (Carabineiro et al. 2011). The lower pH_{PZC} of MMB indicated that the adsorbent surface was more negatively charged compared to BC, suggesting higher adsorption capacity for three FQs owing to potential increased electrostatic interaction. The saturation magnetization value of MMB is 9.8 emu/g (Fig. S3). The low saturation magnetization may be due to the existence of MnO_x (Luo et al. 2013). However, it is enough for magnetic separation in 8 S from water by a magnet (Luo et al. 2013; Yang et al. 2017).

Adsorptive and oxidative interactions between MMB and FQs

The impregnation of Mn-oxides can change the surface properties of BC on which not only adsorption but also oxidation of different adsorbates may take place. There is a long history of studies demonstrating the oxidation of organic compounds following reaction with Mn-oxides. In order to explore the oxidation between three FQs and MMB in the water, UV spectra and HPLC method of the three FQ solutions before and after adsorption at different times (0.17, 0.3, 1, 2, 4 h) are shown in Figs. S4 and S5. The intensity of the CIP, ENR, and NOR peaks at 272, 270, and 273 nm became lower after adsorption. When the results are compared, they can be seen that no obvious additional peaks appear after adsorption at different times. The EDS elemental analysis showed that the content of manganese elements on the surface of biochar was only 4.4%. Compared with pure manganese oxides, the oxidizing ability of MMB is weaker during the removal of FQs (Xiao et al. 2013). Another possible reason is that the oxidation products which produced during the degraded process of three FQs by MMB in the water were adsorbed by MMB (Zhang and Huang 2005). Thus, we focused on the adsorption ability of MMB to FQs in the following study.

Adsorption capacity of BC, FB, and MMB

The BC, FB, and MMB were used to remove three FQs from water. As shown in Fig. 3, the adsorption capacity of three FQs on adsorbents was in the order of MMB > FB > BC. The adsorption capacity of CIP for MMB was 1.56 and 1.87 times

that of FB and BC, respectively. The adsorption capacity for ENR was 1.56 and 1.92 times that of FB and BC, and the adsorption capacity for NOR was 1.53 and 1.80 times that of FB and BC, respectively. The results turned out that the MMB could highly remove three FQs from water than BC and FB.

Effect of contact time and adsorption kinetics

The effect of reaction time on three FQs' removal and adsorption capacities of BC and MMB are depicted in Fig. 4. The adsorption of three FQs rapidly increased in the initial stage, followed by a slow increase until reaching the adsorption equilibrium. The MMB has a better uptake efficiency and removal capacity for three FQs in comparison with the BC. They can be explained by the increase in surface functionalities that are capable of binding with fluoroquinolone antibiotic molecule (Liu et al. 2011). The pseudo-first-order and the pseudo-second-order models are fitted in Fig. S6 and the model parameters are shown in Table 3. The equations are given in Eqs. (3) and (4), respectively.

$$\ln(q_e - q_t) = \ln q_e - k_1 t \tag{3}$$

$$\frac{t}{q_t} = \frac{1}{k_2 q_e^2} + \frac{1}{q_e} t \tag{4}$$

where q_e and q_t are the amount of FQs adsorbed per unit mass of the adsorbent (mg·g⁻¹) at equilibrium and time t ,

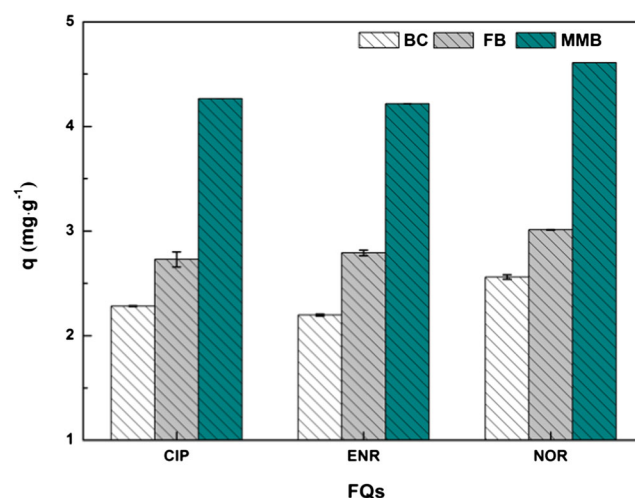


Fig. 3 Adsorption capacity of three FQs by BC, FB, and MMB

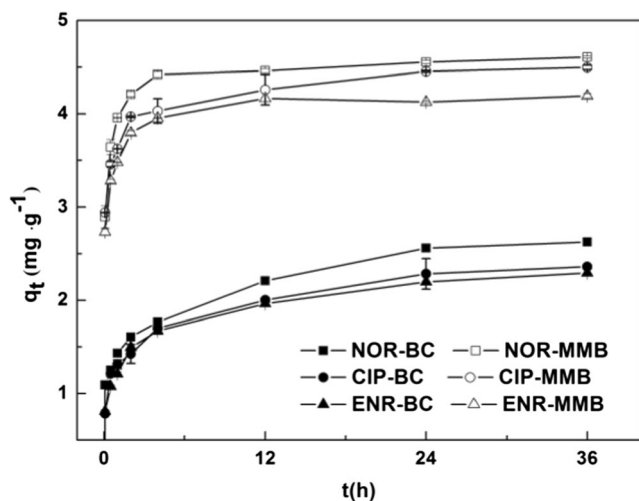


Fig. 4 Equilibrium time of three FQs adsorbed onto BC and MMB

respectively. k_1 (min^{-1}) and k_2 ($\text{g}\cdot\text{mg}^{-1}\cdot\text{min}^{-1}$) are the pseudo-first-order and pseudo-second-order rate constant, respectively. The values of $q_{e(\text{theo})}$, correlation coefficient (R^2), and experimental values of $q_{e(\text{exp})}$ were calculated.

As the results showed, the R^2 values of the pseudo-second-order model were higher than those of the pseudo-first-order model and much closer $q_{e(\text{theo})}$ value to the $q_{e(\text{exp})}$ value when comparing with the pseudo-first-order model, indicating chemisorption played a dominant role in the adsorption process (Kim et al. 2013). To further analyze the diffusion process of three FQs from aqueous solutions to MMB and BC, the kinetic data was fitted with intra-particle diffusion model, and the equation is given in Eq. (5):

$$q_t = K_d t^{1/2} + L \tag{5}$$

where K_d is the intraparticle diffusion rate constant ($\text{mg}(\text{g}\cdot\text{h}^{0.5})^{-1}$), and the values of L ($\text{mg}\cdot\text{g}^{-1}$) depict the thickness of the boundary layer. The values of K_d and L can be obtained by plotting q_t against $t^{0.5}$. Figure 5 shows that the plots for MMB or BC of three FQs have three distinct regions. The sharp first linear portion represents external mass diffusion. The second linear portion represents intraparticle diffusion and the third linear portion indicates the adsorption–desorption equilibrium

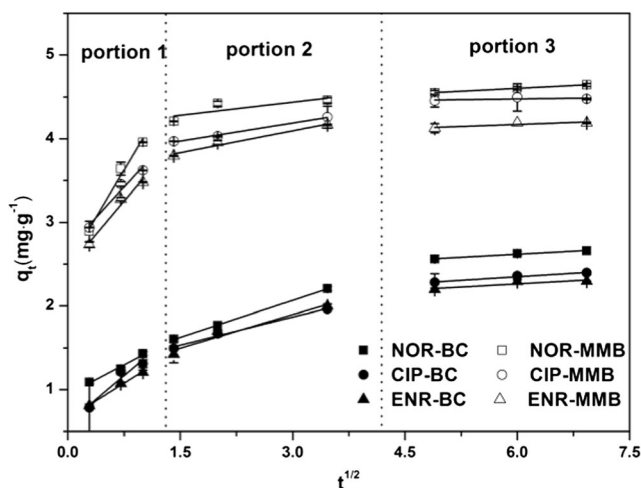


Fig. 5 Intraparticle diffusion plots of three FQs on BC and MMB at 25 °C

(Luo et al. 2013). The rapid initial increase at the first step is due to the availability of free sites on the external surface, as well as the easily accessible sites, in addition to the initial FQ concentration in the solution, while the rate of the followed gradual adsorption step is decreased on the surface and took place within the pores. Meanwhile, the plots do not pass through the origin, suggesting that intraparticle diffusion is not the sole rate-controlling step.

Adsorption isotherm and thermodynamic studies

The adsorption isotherm model is fundamental in describing the reaction behavior between adsorbate and adsorbent (Ueda Yamaguchi et al. 2016). Langmuir model (Eq. (4)) and Freundlich model (Eq. (5)) can be used to fit the experimental equilibrium adsorption data obtained from isotherm studies. In the study, adsorption isotherms of three FQs on MMB and BC for three different temperatures are depicted in Fig. S7, and the calculated adsorption constants are summarized in Table 4.

$$q_e = \frac{Q_{\max}bc_e}{1 + bc_e} \tag{6}$$

$$q_e = k_f c_e^{1/n} \tag{7}$$

Table 3 Kinetic parameters for the adsorption of three FQs onto BC and MMB at 25 °C

Adsorbents	Antibiotics	Pseudo-first-order kinetics			Pseudo-second-order kinetics		
		k_1 (h^{-1})	q_e ($\text{mg}\cdot\text{g}^{-1}$)	R_1^2	k_2 ($\text{g}\cdot(\text{mg}\cdot\text{min})^{-1}$)	q_e ($\text{mg}\cdot\text{g}^{-1}$)	R_2^2
BC	NOR	0.06	1.33	0.9572	0.30	2.71	0.9978
	CIP	0.13	1.49	0.9424	0.35	2.43	0.9981
	ENR	0.13	1.33	0.9766	0.40	2.33	0.9986
MMB	NOR	0.09	0.75	0.8930	0.96	4.64	0.9999
	CIP	0.08	0.84	0.8619	0.77	4.51	0.9999
	ENR	0.07	0.59	0.7167	1.32	4.20	0.9999

where q_e ($\text{mg}\cdot\text{g}^{-1}$) and C_e ($\text{mg}\cdot\text{L}^{-1}$) are the solid-phase and aqueous-phase concentrations at adsorption equilibrium, respectively. Q_{max} ($\text{mg}\cdot\text{g}^{-1}$) is the maximum adsorption capacity and b the constant related to the affinity. K_f and n are indicators of adsorption capacity and intensity, respectively.

As can be seen from Table 4, it was evident that compared with the Freundlich model, the Langmuir model fits the experiment data reasonably well in view of correlation coefficient R^2 . Thus, monolayer adsorption of three FQs occurs on the MMB or BC that dominated the adsorption process with contributions from heterogeneous adsorption (Yang et al. 2017). The maximum adsorption ability of BC followed the order of $\text{NOR} > \text{CIP} > \text{ENR}$; however, MMB followed the order of $\text{CIP} > \text{ENR} > \text{NOR}$. The parameter b is related to the affinity of the binding sites, which allows comparisons of the affinity of adsorbent toward the adsorbate. MMB had a higher affinity for three FQs than did BC, revealing more functional groups on the surface of MMB comparing with the BC, resulting in having the highest adsorption energy. A comparison of Q_{max} values for FQs with those reported previously using different biochar adsorbents is also shown in Table 5. The MMB here exhibited an excellent adsorption performance.

The thermodynamic parameters can be calculated from three different temperature-dependent adsorption isotherms

(Chen et al. 2017; Luo et al. 2013). The standard Gibbs free energy change (ΔG^0), average standard enthalpy change (ΔH^0), and entropy change (ΔS^0) can be calculated as follows:

$$\Delta G^0 = -RT \ln K^0 \tag{8}$$

$$\ln K^0 = \frac{\Delta S^0}{R} - \frac{\Delta H^0}{RT} \tag{9}$$

where R is the gas constant (8.314 J/mol K) and T is the temperature (K). K^0 is the adsorption equilibrium constant, obtained from the linear plots of $\ln K_d$ ($K_d = q_e/C_e$) versus C_e and extrapolating C_e to zero. ΔH^0 and ΔS^0 can be calculated from the slope and intercept of the linear plot of $\ln K_d$ versus $1/T$.

The values of these parameters are listed in Table 6. The negative values of ΔG^0 indicate the spontaneous nature of the adsorption of three FQs onto the two adsorbents. The ΔG^0 values decrease with increasing temperature, demonstrating that higher spontaneity at higher temperatures (Li et al. 2005). Moreover, the positive ΔH^0 values found for the adsorption of three FQs are an endothermic process (Ocampo-Pérez et al. 2012). The obtained positive ΔS^0 values indicate the affinity between three FQs and two adsorbents, and reflected an increasing randomness during the adsorption process on the solid solution interface (Wang et al. 2017b).

Table 4 Parameters of three FQs’ adsorption isotherms based on Freundlich and Langmuir models

Adsorbents	Antibiotic	T (K)	Langmuir model			Freundlich model		
			Q_{max} ($\text{mg}\cdot\text{g}^{-1}$)	b	R^2	n	K_f	R^2
BC	NOR	288	5.29	0.19	0.9939	0.55	1.02	0.9649
		298	5.34	0.24	0.9490	0.53	1.16	0.9087
		308	5.82	0.28	0.9581	0.51	1.43	0.8896
	CIP	288	3.32	0.28	0.9671	0.50	0.83	0.9328
		298	5.22	0.22	0.9711	0.55	1.06	0.9251
		308	5.79	0.22	0.9788	0.56	1.16	0.9537
	ENR	288	3.34	0.23	0.9767	0.50	0.76	0.9150
		298	4.37	0.20	0.9738	0.54	0.87	0.9243
		308	4.41	0.27	0.9350	0.50	1.07	0.8607
MMB	NOR	288	6.52	2.60	0.9694	0.29	4.18	0.7922
		298	6.63	3.39	0.9447	0.29	4.51	0.7879
		308	6.94	3.62	0.9462	0.31	4.88	0.8392
	CIP	288	5.77	3.17	0.9599	0.29	3.88	0.8030
		298	6.94	2.37	0.9003	0.35	4.36	0.8100
		308	8.37	2.20	0.9580	0.35	5.27	0.8586
	ENR	288	6.48	2.40	0.9241	0.31	4.06	0.7800
		298	6.83	2.61	0.9338	0.33	4.39	0.8100
		308	7.19	2.77	0.9157	0.33	4.74	0.8020

Table 5 Comparison of the FQs' adsorption capacities with different biochar adsorbents in the literature

Adsorbents	FQs	Q_{\max} (mg·g ⁻¹)	References
Cassava waste biochar	Norfloxacin	1.67	Luo et al. 2018
KOH-modified cassava waste biochar	Norfloxacin	5.00	Luo et al. 2018
Cassava residue-derived biochar	Ofloxacin	3.00(± 0.1)	Huang et al. 2018
Clay-biochar	Norfloxacin	5.24	Li et al. 2017a, b
Iron-doped activated alumina	Norfloxacin	6.89	Liu et al. 2011
Nano graphene oxide-magnetite	Ciprofloxacin	2.22	Alicanoglu and Sponza 2017
Modified coal fly ash	Ciprofloxacin	1.55	Zhang et al. 2011
Potato stems and leaves biochar (BC)	Norfloxacin	5.82	Present work
	Ciprofloxacin	5.79	Present work
	Enrofloxacin	4.41	Present work
Manganese oxide-loaded magnetic biochar (MMB)	Norfloxacin	6.94	Present work
	Ciprofloxacin	8.37	Present work
	Enrofloxacin	7.19	Present work

pH effects on three fluoroquinolone antibiotics' adsorption

The effect of initial solution pH on three FQs' adsorption by BC and MMB is illustrated in Fig. 6. It could be found out that the overall trend of the impact of initial solution pH on three FQs' adsorption was similar using the same adsorbent. MMB exhibited better adsorption capacity and the maximum adsorption occurs at pH 3.0. The three FQs' adsorption by MMB decreased gradually as pH rises. For BC, the adsorption capacity for NOR and ENR slightly increases with the rise in pH

from 3.0 to 6.0, then, the adsorption capacity decreases gradually with increasing pH from 6.0 to 10.0.

The pH can affect the ionization forms of three FQ molecules in solution. These three FQs have two different pKa values (NOR—pKa₁ = 6.2/pKa₂ = 8.5, CIP—pKa₁ = 6.2/pKa₂ = 8.8; and ENR—pKa₁ = 6.1/pKa₂ = 7.7); when solution pH < pKa₁, three FQs can exist as cationic form. When solution pH are between pKa₁ and pKa₂, they can exist as zwitterionic and in the formation of anionic when pH is above pKa₂. The equilibrium pH values of BC and MMB are presented in Fig. 7. For MMB, when the equilibrium pH values < pH_{PZC},

Table 6 Thermodynamic parameters for the adsorption of three FQs onto adsorbents under different temperatures

Adsorbent		T (K)	Ln <i>k_d</i>	Δ <i>G</i> ⁰ (kJ·mol ⁻¹)	Δ <i>H</i> ⁰ (kJ·mol ⁻¹)	Δ <i>S</i> ⁰ (kJ·mol ⁻¹ ·K ⁻¹)
BC	NOR	288	6.78	-16.23	16.97	0.1153
		298	7.03	-17.42		
		308	7.24	-18.54		
	CIP	288	6.59	-15.78	16.69	0.1131
		298	6.94	-17.19		
		308	7.04	-18.03		
	ENR	288	6.44	-15.42	17.68	0.1149
		298	6.67	-16.53		
		308	6.92	-17.72		
MMB	NOR	288	9.12	-21.84	18.12	0.1389
		298	9.44	-23.39		
		308	9.61	-24.61		
	CIP	288	9.23	-22.10	10.34	0.1127
		298	9.39	-23.26		
		308	9.51	-24.35		
	ENR	288	9.19	-22.00	11.07	0.1148
		298	9.35	-23.17		
		308	9.49	-24.30		

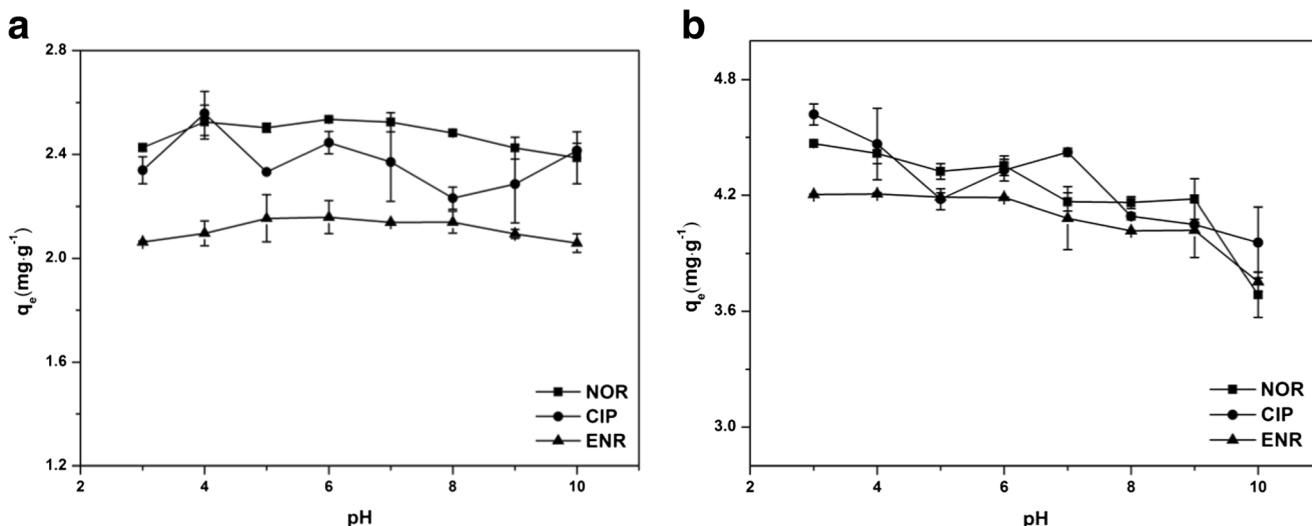


Fig. 6 Effect of initial solution pH on the adsorption of three FQs on BC (a) and MMB (b)

the surface charge of the MMB is positive. At the same time, when the equilibrium $\text{pH} < \text{pK}a_1$ (NOR, CIP, and ENR), cationic form is the dominant species in three FQ solutions. Under this condition, three FQs' adsorption on MMB at low pH can be explained by π - π electron donor-acceptor (EDA) (which includes the cation- π bonding) interactions between the three FQ molecules and adsorbent surface (Kang et al. 2011). When equilibrium $\text{pH} > \text{pH}_{\text{PZC}}$, the adsorption capacity decreased due to zwitterionic interactions as the major factor on the adsorption of three FQs onto MMB (Rajapaksha et al. 2014). Possible mechanisms for three FQs' adsorption on MMB are that the increase in equilibrium pH led to high hydrophilicity and low hydrophobic interactions occur and increased the formation of water clusters and restrained the formation of hydrogen bond, which might have reduced the adsorption between three FQs and MMB (Kang et al. 2011; Wang et al. 2017b; Yang et al. 2017). Furthermore, it could be

observed that the MMB obtained the better adsorption capacity at pH 3.0. It is similar to the results of a previous study (Rajapaksha et al. 2014; Yang et al. 2017).

It could be found out that the surface of BC is positively charged due to the equilibrium pH values lower than pH_{PZC} (Peng et al. 2015), while the equilibrium $\text{pH} > \text{pK}a_2$ (NOR, CIP, and ENR), the anionic form of three FQs is the dominant species in solutions, which indicated that the electrostatic attraction may be one of the mechanisms in the adsorption of three FQs on BC.

Effect of ionic strength

Most wastewater contains a certain amount of salt, which may affect the removal of FQs. Thus, the effect of ionic strength on the adsorption of FQs onto BC and MMB was carried out via a series of experimental studies by adjusting the additive amount of CaCl_2 in the range of 0.001, 0.01, and 0.1 M and at pH value of 3.0. High ionic strength led to a slight decrease in the adsorption of three FQs onto BC and MMB (Fig. S8). This is likely due to the combination of Ca^{2+} and Cl^- ions with the cationic FQs in the solutions, which inhibits the effective contact between the three FQs and adsorbent's surface (Li et al. 2010).

FTIR analysis

The FTIR spectra of BC and MMB are shown in Fig. 8a. For BC, the peaks at 3696 (3422), 1588, 1421, and 874 cm^{-1} are ascribed to the vibration of -OH, C=C, or C=O and carboxyl O=C-O, C-H (Lian et al. 2015; Tang et al. 2016, Sharma et al. 2017), respectively. Compared with BC, the peaks of MMB at 3696 cm^{-1} (-OH) diminished, and the C=C or C=O stretching band shifted from 1588 cm^{-1} for BC to 1567 cm^{-1} , and the carboxyl O=C-O stretching band shifted from 1421 cm^{-1} for

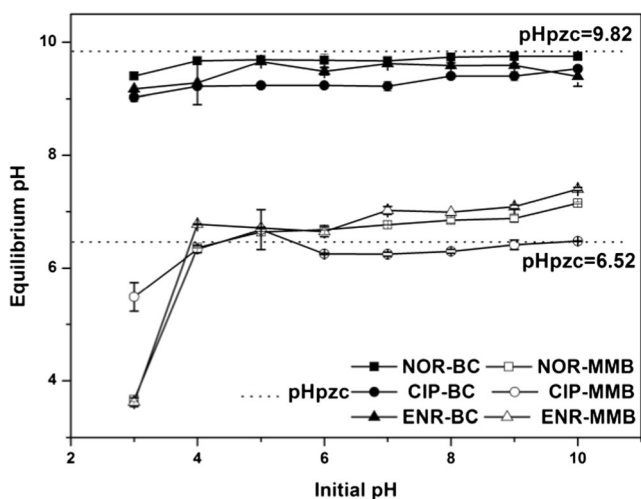


Fig. 7 The equilibrium pH versus the initial pH on the adsorption of three FQs on BC and MMB

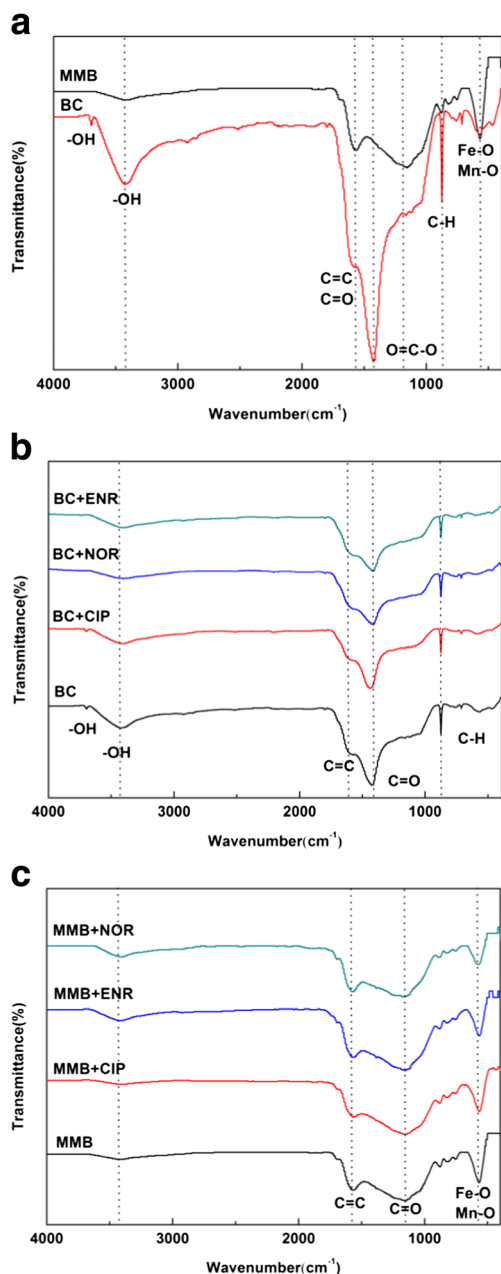


Fig. 8 **a** FTIR spectra for BC and MMB, **b** FTIR spectra of BC before and after three FQs adsorption, and **c** FTIR spectra of MMB before and after three FQs' adsorption

BC to 1156 cm^{-1} for MMB. In addition, the peaks around $400\text{--}800\text{ cm}^{-1}$ that represented the vibrations of Fe–O and Mn–O of MMB are consistent with the results of a previous study (Yang et al. 2017; Zhao et al. 2016).

The FTIR spectra of BC and MMB before and after adsorption are presented in Fig. 8b and c. These peaks had a slight red-shift respectively in three FQs' adsorbed BC and MMB. It could be speculated that these groups may participate in the three FQs' adsorption reaction. In Fig. 8b, the shift of these bands (C=C, C=O, and carboxyl O=C–O) and the decrease of C–H band indicated the significant role of $\pi\text{--}\pi$

interactions between FQs and adsorbents in the adsorption processes (Tang et al. 2016). The peaks centered at 3422 and 3419 cm^{-1} (–OH) weakened, which indicated important hydrogen-bonding interactions. In Fig. 8c, after adsorption with three FQs, the band of Fe–O or Mn–O decreased greatly, which confirmed that the Fe–O or Mn–O provides more adsorption sites in the adsorption processes. And the shift of peaks 1156 cm^{-1} and 1567 cm^{-1} showed the $\pi\text{--}\pi$ interactions between FQs and MMB during the adsorption processes.

Regeneration study

To ensure economic feasibility of the adsorbent, it is necessary to test the regeneration of the adsorbent. The regenerated MMB was subjected to successive adsorption–regeneration. When MMB was initially used for adsorption, the adsorption percentages were about 92%, 91%, and 91% for NOR, CIP, and ENR, respectively. After the first cycle, they presented a slight increase and the adsorption percentage of NOR, CIP, and ENR were 98%, 98%, and 97%, respectively (Fig. S9). This might be related to the surface property changes, including surface area and pore volume that occurred in MMB during the thermal regeneration process (Wei et al. 2013; Wu et al. 2005). It was observed that the adsorption percentage of MMB increased first and then kept constant, after three cycles, the adsorption percentage of NOR, CIP, and ENR onto the recycled MMB still remained at 95%, 98%, and 97%. This result indicated that it could be applied as an effective adsorbent for more cycles by the method of thermal regeneration. These results suggested that the MMB could be applied as an efficient and potential adsorbent for three FQs' removal due to the excellent regeneration performance.

Conclusions

Manganese oxide–loaded magnetic biochar composite (MMB), a novel and bio-based adsorbent, was synthesized successfully. The MMB exhibited a better adsorption capacity than the raw biochar. The maximum adsorption abilities of MMB for NOR, CIP, and ENR were 6.94 , 8.37 , and $7.19\text{ mg}\cdot\text{g}^{-1}$ at 308 K , respectively. In comparison to BC, the adsorption abilities of MMB increased 1.2, 1.5, and 1.6 times for NOR, CIP, and ENR, respectively.

The adsorption of three FQs by two kinds of materials, the MMB with high surface area and pore volume, was compared and also could be easily separated from water under magnetic field, facilitating its application for adsorbing fluoroquinolone antibiotics from water. The solution pH, ionic strength, and temperature had an apparent effect on the adsorption ability of MMB. In addition, the adsorbent of MMB could be regenerated and reused. Thus, MMB could be a potential adsorbent for fluoroquinolone antibiotics in aquatic environments.

Acknowledgements This work was supported by Gansu Natural Science Fund, China (17JR5RA218) and the Fundamental Research Funds for the Central Universities at Lanzhou University (lzujbky-2017-212, lzujbky-2015-184).

References

- Alicanoglu P, Sponza DT (2017) Removal of ciprofloxacin antibiotic with nano graphene oxide magnetite composite: comparison of adsorption and photooxidation processes. *Desalin Water Treat* 63:293–307
- Carabineiro SA, Thavorn-Amornsri T, Pereira MF, Figueiredo JL (2011) Adsorption of ciprofloxacin on surface-modified carbon materials. *Water Res* 45:4583–4591
- Chen L, Feng S, Zhao D, Chen S, Li F, Chen C (2017) Efficient sorption and reduction of U(VI) on zero-valent iron-polyaniline-graphene aerogel ternary composite. *J Colloid Interface Sci* 490:197–206
- Conkle JL, Latta C, White JR, Cook RL (2010) Competitive sorption and desorption behavior for three fluoroquinolone antibiotics in a wastewater treatment wetland soil. *Chemosphere* 80(11):1353–1359
- Fan Z, Zhang Q, Li M, Niu D, Sang W, Verpoort F (2018) Investigating the sorption behavior of cadmium from aqueous solution by potassium permanganate-modified biochar: quantify mechanism and evaluate the modification method. *Environ Sci Pollut Res Int* 7:1–10
- Han R, Zou W, Zhang Z, Shi J, Yang J (2006) Removal of copper(II) and lead(II) from aqueous solution by manganese oxide coated sand. I. Characterization and kinetic study. *J Hazard Mater* 137(1):384–395
- Huang P, Ge C, Feng D, Yu H, Luo J, Li J, Strong PJ, Samah AK, Bolan NS, Wang H (2018) Effects of metal ions and pH on ofloxacin sorption to cassava residue-derived biochar. *Sci Total Environ* 616-617:1384–1391
- Kang J, Liu H, Zheng YM, Qu J, Chen JP (2011) Application of nuclear magnetic resonance spectroscopy, Fourier transform infrared spectroscopy, UV-visible spectroscopy and kinetic modeling for elucidation of adsorption chemistry in uptake of tetracycline by zeolite beta. *J Colloid Interface Sci* 354:261–267
- Khmeleva TN, Georgiev TV, Jasieniak M, Skinner WM, Beattie DA (2005) XPS and ToF-SIMS study of a chalcopyrite-pyrite-sphalerite mixture treated with xanthate and sodium bisulphite. *Surf Interface Anal* 37:699–709
- Kim EJ, Lee CS, Chang YY, Chang YS (2013) Hierarchically structured manganese oxide-coated magnetic nanocomposites for the efficient removal of heavy metal ions from aqueous systems. *ACS Appl Mater Interfaces* 5:9628–9634
- Kong X, Liu Y, Pi J, Li W, Liao Q, Shang J (2017) Low-cost magnetic herbal biochar: characterization and application for antibiotic removal. *Environ Sci Pollut Res* 24:6679–6687
- Kumar A, Sharma G, Kalia S, Guo C, Mu N (2017) Facile hetero-assembly of superparamagnetic Fe₃O₄/BiVO₄ stacked on biochar for solar photo-degradation of methyl paraben and pesticide removal from soil. *J Photochem Photobiol A Chem* 337:118–131
- Li B, Yang L, Wang CQ, Zhang QP, Liu QC, Li YD, Xiao R (2017b) Adsorption of Cd(II) from aqueous solutions by rape straw biochar derived from different modification processes. *Chemosphere* 175:332–340
- Li Y, Wang Z, Xie X, Zhu J, Li R, Qin T (2017a) Removal of norfloxacin from aqueous solution by clay-biochar composite prepared from potato stem and natural attapulgite. *Colloids Surf A Physicochem Eng Asp* 514:126–136
- Li YH, Di Z, Ding J, Wu D, Luan Z, Zhu Y (2005) Adsorption thermodynamic, kinetic and desorption studies of Pb²⁺ on carbon nanotubes. *Water Res* 39:605–609
- Li Z, Schulz L, Ackley C, Fenske N (2010) Adsorption of tetracycline on kaolinite with pH-dependent surface charges. *J Colloid Interface Sci* 351:254–260
- Lian F, Sun B, Chen X, Zhu L, Liu Z, Xing B (2015) Effect of humic acid (HA) on sulfonamide sorption by biochars. *Environ Pollut* 204:306–312
- Liu W, Zhang J, Zhang C, Ren L (2011) Sorption of norfloxacin by lotus stalk-based activated carbon and iron-doped activated alumina: mechanisms, isotherms and kinetics. *Chem Eng J* 171:431–438
- Luo C, Tian Z, Yang B, Zhang L, Yan S (2013) Manganese dioxide/iron oxide/acid oxidized multi-walled carbon nanotube magnetic nanocomposite for enhanced hexavalent chromium removal. *Chem Eng J* 234:256–265
- Luo J, Xue L, Ge C, Müller K, Yu H, Peng H, Li J, Tsang DCW, Bolan NS, Wang H (2018) Sorption of norfloxacin, sulfamerazine and oxytetracycline by KOH-modified biochar under single and ternary systems. *Bioresour Technol* 263:385–392
- Ocampo-Pérez R, Rivera-Utrilla J, Gómez-Pacheco C, Sánchez-Polo M, López-Peñalver JJ (2012) Kinetic study of tetracycline adsorption on sludge-derived adsorbents in aqueous phase. *Chem Eng J* 213:88–96
- Peng B, Liang C, Que C, Ke Y, Fei D, Deng X, Shi G, Xu G, Wu M (2016) Adsorption of antibiotics on graphene and biochar in aqueous solutions induced by π - π interactions. *Sci Rep* 6:31920
- Peng X, Hu F, Lam FL, Wang Y, Liu Z, Dai H (2015) Adsorption behavior and mechanisms of ciprofloxacin from aqueous solution by ordered mesoporous carbon and bamboo-based carbon. *J Colloid Interface Sci* 460:349–360
- Peng X, Liu X, Zhou Y, Peng B, Tang L, Luo L, Yao B, Deng Y, Tang J, Zeng G (2017) New insights into the activity of a biochar supported nanoscale zerovalent iron composite and nanoscale zero valent iron under anaerobic or aerobic conditions. *RSC Adv* 7:8755–8761
- Rajapaksha AU, Vithanage M, Zhang M, Ahmad M, Mohan D, Chang SX, Ok YS (2014) Pyrolysis condition affected sulfamethazine sorption by tea waste biochars. *Bioresour Technol* 166:303–308
- Sharma G, Naushad M, Kumar A, Rana S, Sharma S, Bhatnagar A, Stadler FJ, Ghfar AA, Khan MR (2017) Efficient removal of Coomassie brilliant blue R-250 dye using starch/poly(alginate-chitosan) nanohydrogel. *Process Saf Environ Prot* 109:301–310
- Solanki A, Boyer TH (2017) Pharmaceutical removal in synthetic human urine using biochar. *Environ Sci Water Res Technol* 3:553–565
- Song Z, Lian F, Yu Z, Zhu L, Xing B, Qiu W (2014) Synthesis and characterization of a novel MnOx-loaded biochar and its adsorption properties for Cu²⁺ in aqueous solution. *Chem Eng J* 242:36–42
- Tan X, Liu Y, Zeng G, Wang X, Hu X, Gu Y, Yang Z (2015) Application of biochar for the removal of pollutants from aqueous solutions. *Chemosphere* 125:70–85
- Tang J, Huang Y, Gong Y, Lyu H, Wang Q, Ma J (2016) Preparation of a novel graphene oxide/Fe-Mn composite and its application for aqueous Hg(II) removal. *J Hazard Mater* 316:151–158
- Ueda Yamaguchi N, Bergamasco R, Hamoudi S (2016) Magnetic MnFe₂O₄-graphene hybrid composite for efficient removal of glyphosate from water. *Chem Eng J* 295:391–402
- Van Doorslaer X, Dewulf J, Van Langenhove H, Demeestere K (2014) Fluoroquinolone antibiotics: an emerging class of environmental micropollutants. *Sci Total Environ* 500-501:250–269
- Wang L, Qiang Z, Li Y, Ben W (2017a) An insight into the removal of fluoroquinolones in activated sludge process: sorption and biodegradation characteristics. *J Environ Sci* 56:263–271
- Wang P, Tang L, Wei X, Zeng G, Zhou Y, Deng Y, Wang J, Xie Z, Fang W (2017b) Synthesis and application of iron and zinc doped biochar for removal of p-nitrophenol in wastewater and assessment of the influence of co-existed Pb(II). *Appl Surf Sci* 392:391–401
- Wei H, Deng S, Huang Q, Nie Y, Wang B, Huang J, Yu G (2013) Regenerable granular carbon nanotubes/alumina hybrid adsorbents

- for diclofenac sodium and carbamazepine removal from aqueous solution. *Water Res* 47:4139–4147
- Wu R, Qu J, Chen Y (2005) Magnetic powder MnO-Fe₂O₃ composite—a novel material for the removal of azo-dye from water. *Water Res* 39: 630–638
- Xiao X, Sun SP, McBride MB, Lemley AT (2013) Degradation of ciprofloxacin by cryptomelane-type manganese(III/IV) oxides. *Environ Sci Pollut Res* 20(1):10–21
- Yang Y, Hu X, Zhao Y, Cui L, Huang Z, Long J, Xu J, Deng J, Wu C, Liao W (2017) Decontamination of tetracycline by thiourea-dioxide-reduced magnetic graphene oxide: effects of pH, ionic strength, and humic acid concentration. *J Colloid Interface Sci* 495:68–77
- Yi S, Sun Y, Hu X, Xu H, Gao B, Wu J (2017) Porous nano-cerium oxide wood chip biochar composites for aqueous levofloxacin removal and sorption mechanism insights. *Environ Sci Pollut Res*:1–9
- Zhao J, Liu J, Li N, Wang W, Nan J, Zhao Z, Cui F (2016) Highly efficient removal of bivalent heavy metals from aqueous systems by magnetic porous Fe₃O₄-MnO₂: adsorption behavior and process study. *Chem Eng J* 304:737–746
- Zhang CL, Qiao GL, Zhao F, Wang Y (2011) Thermodynamic and kinetic parameters of ciprofloxacin adsorption onto modified coal fly ash from aqueous solution. *J Mol Model* 163(1):53–56
- Zhang H, Huang CH (2005) Oxidative transformation of fluoroquinolone antibacterial agents and structurally related amines by manganese oxide. *Environ Sci Technol* 39(12):4474–4483